

Roto-vibrational spectrum and Wigner crystallization in two-electron parabolic quantum dots

Antonio Puente,¹ Llorenç Serra,^{1,2} and Rashid G. Nazmitdinov^{1,3}

¹*Departament de Física, Universitat de les Illes Balears, E-07122 Palma de Mallorca, Spain*

²*Institut Mediterrani d'Estudis Avançats IMEDEA (CSIC-UIB), E-07122 Palma de Mallorca, Spain*

³*Bogoliubov Laboratory of Theoretical Physics, Joint Institute for Nuclear Research, 141980 Dubna, Russia*

(Dated: 19 August, 2003)

We provide a quantitative determination of the crystallization onset for two electrons in a parabolic two-dimensional confinement. This system is shown to be well described by a roto-vibrational model, Wigner crystallization occurring when the rotational motion gets decoupled from the vibrational one. The Wigner molecule thus formed is characterized by its moment of inertia and by the corresponding sequence of rotational excited states. The role of a vertical magnetic field is also considered. Additional support to the analysis is given by the Hartree-Fock phase diagram for the ground state and by the random-phase approximation for the moment of inertia and vibron excitations.

PACS numbers: 73.21.La, 73.21.-b

I. INTRODUCTION

For a low enough electron density, Wigner¹ predicted that electrons should localize creating an ordered spatial structure, thenceforth named a Wigner crystal, that breaks the complete translational symmetry of the homogeneous electron gas (also see Ref. 2). Indeed, the formation of the Wigner crystal was observed in two-dimensional (2D) distributions of electrons on the surface of liquid helium.³ A phase transition, induced by the magnetic field, from an electron liquid to a crystalline structure has also been reported for a 2D electron plasma at a GaAs/AlGaAs heterojunction.⁴

The existence of different phases in quantum dots, where a few electrons are confined into a small space, has become a topical subject in mesoscopic physics (see, for a recent review, Ref. 5). In fact, the high controllability of quantum dots suggests that these systems could provide an attractive opportunity to achieve the appropriate conditions for localized states. It is precisely to stress this controllability that the names *artificial atoms* and *quantum dots* have been coined.

There is a general persuasion that the Wigner crystallization in quantum dots, whose localized states are referred to as Wigner molecules, should occur at significantly larger densities than in the 2D bulk. It is based on the argument that in quantum dots potential-energy contributions can easily exceed the kinetic terms and, therefore, electronic motion can be effectively quenched by manipulating the external confinement and/or an applied magnetic field. As for the homogeneous gas, one would expect that in crystallized states the kinetic energy is solely that of the vibrational zero-point motion of the electrons around their mean positions, much smaller than the interaction (potential) energy. Various approaches including ab initio calculations within diffusion and path integral Monte Carlo methods, Hartree-Fock and spin-density functional methods *etc* have been applied to analyze the onset of the crystallization.⁵ However, a non-

ambiguous theoretical result that would justify the above conjecture for a zero magnetic field is lacking. The case with an intense magnetic field is better understood since the magnetic field induces an edge reconstruction, beginning with the appearance of localized vortices on the outer region, that ultimately propagates to all the dot for very high B 's.^{5,6}

In the simpler case of a two-electron 2D quantum dot at zero magnetic field, Yannouleas and Landman⁷ pointed out that the excited-state energies of this system closely follow the rotor sequence when the repulsion-to-confinement ratio, as given by the Wigner parameter R_W , is large enough (~ 200). This was shown to be a proof of the crystallization of the two electrons on fixed positions in a reference frame which is rotating. Quite remarkably, the hypothesized *rotating Wigner molecule* fulfills at the same time the strict symmetry conditions of quantum mechanics –circularity in this case– and the obvious preference for opposite positions when repulsion is large enough. This is a major difference from the above mentioned bulk case where a Hamiltonian symmetry (translation) is broken by the crystallized state. For Wigner molecules, symmetries are preserved in the laboratory frame and one must consider an intrinsic (rotating) frame to 'see' the underlying deformation. A similar situation is found for particular states of two-electron atoms that have been much investigated in physical chemistry (we address the reader to the review paper by Berry⁸). For the two-electron quantum dot, however, the crystallization condition from Ref. 7, $R_W \sim 200$, looks disappointing since it seems unrealistic to achieve such a value experimentally.

Although the exact ground-state wave function of the two-electron artificial atom can be obtained, at least numerically, it may seem paradoxical that one also needs the excited states in order to ascertain the existence of a crystallization. In fact, this inability to disentangle the system's intrinsic structure from its full wave function in a clear way can be taken as a weakness of the ab initio, symmetry preserving, approaches. In general,

even in cases when the exact ground- and excited-state wave functions and energies are known, an intrinsic deformation can only be inferred by comparing with the result of simpler models in which either symmetries are relaxed or the intrinsic structure is imposed. A clear example of the former approach is given by the unrestricted Hartree-Fock (HF) method for the ground state^{9,10} followed by the random-phase approximation (RPA) for excitations.¹¹ Conversely, the roto-vibrational model of Wendler *et al.*¹² for two electrons in a ring could be included in the latter category.

One should be aware that when symmetries are relaxed, as in the Hartree-Fock approach, artifacts or unphysical properties may appear. In a recent contribution Reusch and Grabert¹³ discussed the validity of the latter, drawing special attention to the caution with which one must take Hartree-Fock predictions on symmetry breaking, in agreement with the results presented below. Therefore, a complete physical understanding requires both exact results and model solutions. This way the system's intrinsic deformations are physically understood while, at the same time, artifacts can be safely discarded. A paradigmatic case where the proposed analysis can be performed is given by the two-electron 2D parabolic quantum dot. The separation of center-of-mass and relative coordinates along with the circular symmetry restriction allows the reduction of the multidimensional Schrödinger equation to just a radial one, easily solvable numerically. On the other hand, the Hartree-Fock and RPA solutions without any symmetry restriction can also be obtained. A most convenient basis for this latter calculations is given by the Fock-Darwin orbitals in terms of which one can analytically develop much of the required algebra. It is our aim in this work to determine the crystallization onset of two-electron parabolic dots by recourse to the three different approaches referred to above; namely, (a) an analytical roto-vibrational model, (b) a numerical solution of the Schrödinger equation, and (c) symmetry unrestricted Hartree-Fock and random-phase approximations.

Hereafter, we refer to the solution of the Schrödinger equation for the two-electron parabolic dot as the *exact* solution. It should be pointed out that, as shown by Taut,¹⁴ this Schrödinger equation is analytically solvable only for particular confinement/interaction strengths. For general values of this quantity a numerical treatment is required. As mentioned above, the most straightforward one is an integration of the radial equation^{7,15} but, nevertheless, other methods such as diagonalization in a basis^{16,17} and the Monte Carlo method^{18,19} have also been applied. One of us has used the so-called oscillator representation method, perturbatively treating the residual interaction, to derive analytical expressions for the energy levels.²⁰

The paper is organized as follows. Section II introduces the magneto-parabolic units that allow one to trace the evolution of ground and excited states of artificial atoms at various conditions. An analytical roto-vibrational

model for the two-electron parabolic quantum dot is described in Sec. III. Section IV provides details of our numerical calculation of exact solutions and compares these solutions with those of the roto-vibrational model. Section V analyzes the reliability of the Hartree-Fock and RPA results for the present system. A short summary is finally drawn in Sec. VI.

II. MAGNETO-PARABOLIC UNIT SYSTEM

We consider two electrons with a Coulomb interaction between them. The electrons move in the xy plane where a circular parabolic confinement induces the formation of an electron island. The system is also subject to an external magnetic field applied in the vertical direction (z). The full Hamiltonian thus reads

$$\mathcal{H} = \sum_{i=1,2} \left[\frac{1}{2m} \left(\mathbf{p} + \frac{e}{c} \mathbf{A} \right)^2 + \frac{1}{2} m \omega_0^2 r^2 \right]_i + \frac{e^2}{\kappa r_{12}} + g^* \mu_B B S_z. \quad (1)$$

In Eq. (1), m , κ , and g^* are the electron's effective mass, the dielectric constant, and the effective gyromagnetic factor, respectively, and we have used planar polar coordinates ($r^2 = x^2 + y^2$). The two contributions within the square brackets are, respectively, the generalized kinetic energy in terms of the vector potential \mathbf{A} , and the external confinement. Within the so-called symmetric gauge one has $\mathbf{A}(x, y) = B/2(-y, x)$. The next contribution is the Coulomb repulsion and, finally, the last term is the Zeeman energy involving the total spin operator S_z and the universal Bohr's magneton $\mu_B = e\hbar/2m_e c$.

It is well known that in the chosen gauge the magnetic field contributions can be recast into the form of an effective parabolic confinement of frequency $\Omega = \sqrt{\omega_0^2 + \omega_c^2/4}$, where $\omega_c = eB/mc$ is the cyclotron frequency, and an additional angular-momentum-dependent term $(\hbar\omega_c/2)\ell_z$ (cf. Refs. 21,22). The magneto-parabolic units (mpu) we shall use consist of taking $\hbar\Omega$ as the energy unit and $\ell_\Omega \equiv \sqrt{\hbar/(m\Omega)}$ as the length unit. In addition, one also imposes \hbar as angular momentum unit which, in turn, fixes the time unit $\tau_\Omega = 1/\Omega$. Summarizing in the standard abuse of notation we may write $\hbar = \Omega = \ell_\Omega = 1$ mpu. This is a natural choice for magneto-parabolic confinements and it allows one to express the spatial part of the Hamiltonian in terms of only two adimensional parameters, namely,

$$R_{mp} = \frac{e^2/(\kappa\ell_\Omega)}{\hbar\Omega}, \quad (2)$$

$$W_{mp} = \frac{\omega_c}{\Omega}. \quad (3)$$

Note that R_{mp} and W_{mp} give, respectively, the ratios of Coulomb interaction strength and cyclotron frequency to effective confinement. In the absence of a magnetic field R_{mp} coincides with the so-called Wigner parameter

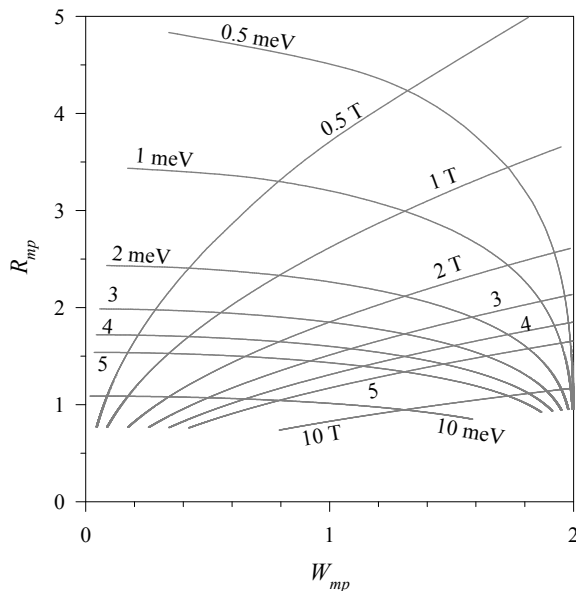


FIG. 1: Equivalence between the mpu pair of adimensional parameters (R_{mp}, W_{mp}) and the physical values of the external parabolic strength and magnetic field ($\hbar\omega_0, B$). The bulk GaAs effective mass $m = 0.067m_e$ and dielectric constant $\kappa = 12.4$ have been assumed.

R_W of Ref. 7. Also note that W_{mp} has a maximal value $W_{mp} = 2$ that corresponds to a zero confinement $\omega_0 = 0$. We also mention that Reusch and Grabert used these parameters in their recent Hartree-Fock calculations.¹³

Within the mpu system the Hamiltonian reads

$$\mathcal{H} = \sum_{i=1,2} \left[-\frac{1}{2}\nabla^2 + \frac{1}{2}r^2 + \frac{W_{mp}}{2}\ell_z \right]_i + \frac{R_{mp}}{r_{12}} + \frac{g^*m^*}{2}W_{mp}S_z, \quad (4)$$

where m^* is the adimensional ratio of effective to bare electron mass, i.e., $m^* = m/m_e$. The passage from the mpu system, with a given R_{mp} and W_{mp} , to physical units requires the knowledge of the effective mass m and the dielectric constant κ . More specifically, with fixed m and κ one can invert Eqs. (2) and (3) for the effective confinement Ω and cyclotron ω_c frequencies or, equivalently, for the external confinement ω_0 and the magnetic field B . In terms of these results the physical values of the energy ($\hbar\Omega$) and length (ℓ_Ω) units are readily found.

Figure 1 shows the equivalence between the adimensional parameters (R_{mp}, W_{mp}) of the mpu Hamiltonian and the physical values of ($\hbar\omega_0, B$) for the case of a GaAs host semiconductor having $m = 0.067m_e$ and $\kappa = 12.4$. The advantage of working with the mpu system becomes obvious when realizing that, with unit redefinition, the same numerical results can be equally applied to a variety of confinements, magnetic fields, and material parameters (effective mass and dielectric constants). Therefore, the model acquires a certain degree of universality. We also expect that quantum dot properties such as scaling

laws or phase diagrams will be better displayed in terms of the adimensional mpu parameters.

III. A ROTO-VIBRATIONAL MODEL

Taking Eq. 4 as a starting point and introducing the standard center of mass (R, Θ) and relative (r, θ) coordinates it is well known that the Hamiltonian separates and, therefore, that the wave function factorizes. The center of mass (CM) problem is that of a single particle in a harmonic potential and magnetic field, having an analytical solution in terms of Fock-Darwin orbitals and energies $\varepsilon_{NM}^{(CM)} = 2N + |M| + 1 + MW_{mp}/2$, with (N, M) the radial and angular momentum center-of-mass quantum numbers. Focusing next on the relative problem, one introduces the wave function $e^{im\theta}u_{nm}(r)/\sqrt{r}$ having good ℓ_z angular momentum (m), and an additional quantum number n whose meaning will be clarified below. The equation for the unknown $u_{nm}(r)$ reads

$$u_{nm}'' + \left[\tilde{\varepsilon}_{nm}^{(rm)} - \left(\frac{1}{4}r^2 + \frac{R_{mp}}{r} + \frac{m^2 - 1/4}{r^2} \right) \right] u_{nm} = 0, \quad (5)$$

where we have defined $\tilde{\varepsilon}_{nm}^{(rm)} = \varepsilon_{nm}^{(rm)} - mW_{mp}/2$ in terms of the relative-motion energy $\varepsilon_{nm}^{(rm)}$ and the mpu parameter W_{mp} .

Equation (5) will be the basis of our roto-vibrational model. Note that it resembles a Schrödinger one-dimensional equation with an effective potential

$$V_{eff}(r) = \frac{1}{4}r^2 + \frac{R_{mp}}{r} + \frac{m^2 - 1/4}{r^2} \quad (6)$$

that includes the rotational motion term $\sim m^2/r^2$ characterized by the angular momentum quantum number m . We can expect a rigid-rotor behaviour if $V_{eff}(r)$ has a deep minimum at a particular value $r = r_0$. When this occurs the situation resembles that of diatomic molecules like H_2 , where the potential well for nuclear motion is described by the Morse potential (see Ref. 23). In the present case the effective potential indeed has a minimum although it is in general rather shallow. This property is responsible for the coupling between rotation and vibration or, equivalently, for the *floppiness* of the rotating molecule mentioned in Ref. 7.

The minimum condition on $V_{eff}(r)$ yields the rotor radius from

$$\frac{r_0}{2} - \frac{R_{mp}}{r_0^2} - \frac{2(m^2 - 1/4)}{r_0^3} = 0. \quad (7)$$

Neglecting the third contribution on the left-hand-side, an assumption that will be valid for large enough r_0 , one finds the asymptotic law $r_0 \approx (2R_{mp})^{1/3}$. Now, expanding to second order around r_0 we approximate

$$\begin{aligned} V_{eff}(r) &\approx V_{eff}(r_0) + \frac{1}{2} \left(\frac{3}{2} + 2\frac{m^2 - 1/4}{r_0^4} \right) (r - r_0)^2 \\ &= const. + \frac{1}{2}k(r - r_0)^2, \end{aligned} \quad (8)$$

a result that, when substituted into Eq. (5) for the round parentheses, leads immediately to the analytical prediction²⁴

$$\begin{aligned} \tilde{\varepsilon}_{nm}^{(\text{rm})} &= \frac{1}{4}r_0^2 + \frac{R_{mp}}{r_0} + \frac{m^2 - 1/4}{r_0^2} \\ &+ \left(n + \frac{1}{2}\right) \sqrt{3 + 4\frac{m^2 - 1/4}{r_0^4}}. \end{aligned} \quad (9)$$

The result embodied by Eq. (9) has a clear physical interpretation. It contains a rotor-like contribution, $\sim m^2/(2\mathcal{J})$, with a moment of inertia given by $\mathcal{J} = r_0^2/2$ mpu, and a vibrational one characterized by a quantum number n . The vibrational frequency $\omega_{vib} = \sqrt{k/\mu}$ ($\mu = 1/2$) is given by the last square-root factor. Similar to atomic molecules, there is roto-vibrational coupling, since the vibration frequency depends on m and, in addition, centrifugal distortion since r_0 also depends on m . For large enough values of R_{mp} , implying large r_0 and therefore small average densities, the centrifugal distortion disappears and one has $r_0 \approx (2R_{mp})^{1/3}$ for all m 's. In this limit rotational terms become negligible, as well as roto-vibrational ones. Thus, Eq. (9) reduces to a simple m -independent asymptotic expression

$$\tilde{\varepsilon}_n^{(\text{rm})} = \frac{3}{2^{4/3}}R_{mp}^{2/3} + \sqrt{3} \left(n + \frac{1}{2}\right). \quad (10)$$

When adding the magnetic field, the roto-vibrational energy becomes

$$\begin{aligned} \varepsilon_{nm}^{(\text{rm})} &= \tilde{\varepsilon}_{nm}^{(\text{rm})} + mW_{mp}/2 \\ &\sim \frac{(m + W_{mp}r_0^2/4)^2}{r_0^2} + \left(n + \frac{1}{2}\right)\omega_{vib}, \end{aligned} \quad (11)$$

in agreement with the expectations from Ref. 12 for two interacting electrons in a quantum ring.²⁵ It is worth stressing that since the W_{mp} dependence only amounts to an energy shift of the Eq. (5) eigenvalue, the radial function $u_{nm}(r)$ does not depend on W_{mp} . Therefore, one may conclude that the roto-vibrational properties are not affected by magnetic fields, for a fixed (n, m) state. Of course, since the energy shift varies for different states, the magnetic field will modify the ordering of energy levels. For instance, the level crossings as a function of W_{mp} will cause the ground state to have a nonvanishing m -value. This actually explains the buildup of increasing permanent currents in the dot's ground state.

The results from this section will be validated by comparing with the exact ones below. The roto-vibrational model presented here allows one to determine the crystallization onset from the criterion that rotation and vibration motions decouple when intrinsic-frame electron localization sets in. Conversely, when the coupling is strong the system could be represented by either a vibrating rotor or a rotating vibrator and, therefore, the situation can not be clearly resolved. It is also worth stressing that the roto-vibrational model describes all possible excitations

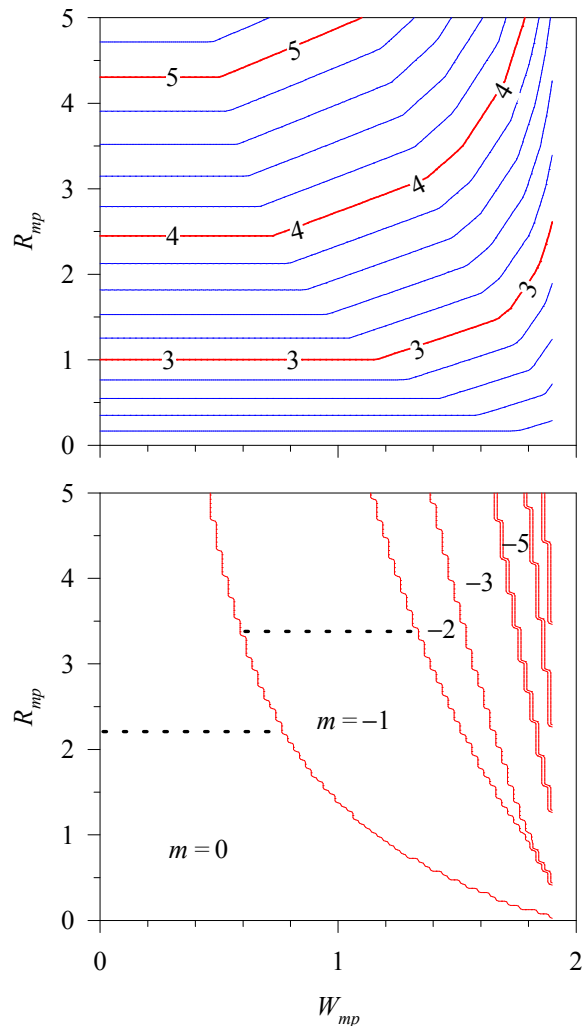


FIG. 2: (Color online) Upper panel: Ground state energy in mpu's for the two electron dot. Lower panel: Ground state relative angular momentum. Note that since $M = 0$, relative and total angular momentum coincide. Even- m (odd- m) regions correspond to singlet (triplet) ground states. Results for $1.9 \leq W_{mp} \leq 2$ are not shown due to the excessively large variations of the computed quantities in this region. The dotted lines separate in each domain with a given m the crystallized (above) from the non crystallized (below) phases using the criterion of roto-vibrational coupling below 3 % (See subject. IV.B).

of the relative-motion problem. For this particular system, this amounts to a description of all the excitations since the center-of-mass and spin degrees of freedom can be analytically integrated out.

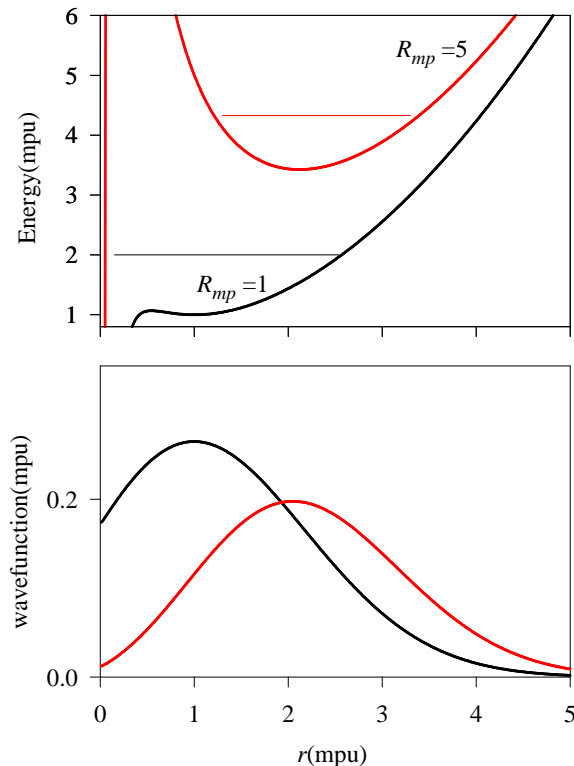


FIG. 3: (Color online) Upper panel: Effective potential defined by Eq. (6) for $m = 0$ and two different values of R_{mp} . The relative-motion eigenenergy $\tilde{\epsilon}_{00}$ is given in each case by the horizontal line. Lower panel: radial eigenfunction $u_{00}(r)/\sqrt{r}$ for the same two potentials of the upper panel.

IV. ONSET OF WIGNER CRYSTALLIZATION

A. Exact solutions

We have solved the radial equation for the relative problem, Eq. (5), numerically. Several standard approaches to eigenvalue problems with boundary conditions can be used for this purpose. Specifically, we have applied the so-called matching method where one integrates with the Numerov or Runge-Kutta algorithms from the origin $r = 0$ outwards assuming an $r^{|m|+1/2}$ behaviour. Additionally, imposing an exponential decay law $\exp(-r^2/4)$ for large r , inwards integration is performed and the two solutions are required to match at an intermediate r -point. To ascertain the numerical result for the eigenvalue, as a control we also used the method of ‘node-counting’, where only outwards integration is performed and the eigenvalue is found from the condition that $u_{nm}(r)$ increases by one the number of radial nodes from the required value when the energy exceeds the correct eigenvalue by an infinitesimal amount. In principle, the node-counting method assures the correct boundary condition at $r \rightarrow \infty$ automatically. However, in practice, there always remains a small difference between the numerical and exact eigenvalues, responsible for a deviation

from the exponential decay from some (large) r onwards. In spite of this possible difference in asymptotic behavior, the two methods (matching and nodecounting) provide to a high accuracy the same eigenvalue.

With the above numerical methods an exploration of a part of the $R_{mp} - W_{mp}$ plane has been performed. Figure 2 summarizes the results for ground-state energy and angular momentum. Note that the ground state always has $(N, M) = (0, 0)$ for the CM quantum numbers and that, because of symmetry, even (odd) m states are associated with singlet (triplet) total spin. Clear singlet-triplet oscillations, as studied in the literature (cf. Ref. 17), are seen in the lower panel of Fig. 2. It is also worth mentioning that the ground-state energy contour lines are piece-wise linear as a result of the simple dependence on the W_{mp} parameter. Indeed, the energy is totally W_{mp} -independent for $m = 0$ and a fixed R_{mp} .

Figure 3 displays the radial wave functions $u_{00}(r)/\sqrt{r}$ for two different values of R_{mp} as well as the corresponding effective potentials V_{eff} defined by Eq. (6). We note that, in agreement with the discussion of the preceding section, when increasing R_{mp} the effective-potential minimum moves outwards and it effectively binds the lower states to its neighborhood. When this occurs the radial probability is strongly quenched at small r (lower panel) and the scenario indeed resembles the familiar one from the physics of diatomic molecules. A more detailed comparison of the roto-vibrational model with the exact results will be done in the next subsection.

B. Crystallization criterion

The validity of the roto-vibrational model presented in Sec. III is proved by the results of Fig. 4. As shown in the upper panel, the error of the analytical prediction for $\tilde{\epsilon}_{nm}$ is important only when R_{mp} is small. As a matter of fact, for $R_{mp} > 2$ the discrepancy for $\tilde{\epsilon}_{00}$ is always below 2%, even with the asymptotic expression Eq. (10). Note that the relative errors slightly increase with increasing n (dashed curves), although the analytical approximation can still be considered quite good. The analogous comparison for $m > 0$ (not shown) yields smaller relative errors than those for $m = 0$. The lower panel of Fig. 4 analyzes the excitation energies as measured from $\tilde{\epsilon}_{00}$, again showing an excellent agreement between the exact results and the ones obtained with the analytical model, with small deviations only at small R_{mp} . Based on the asymptotic expression, Eq. (10), we have chosen $1/R_{mp}^{2/3}$ as an independent variable in order to better display the linear behavior associated with the rigid rotor at large R_{mp} .

We shall rely on the high accuracy of the roto-vibrational model to provide a quantitative measure of the crystallization onset. Our criterion will be the following: the two-electron parabolic system is assumed to be crystallized as a rotating Wigner molecule when the roto-vibrational coupling falls below a given percentage

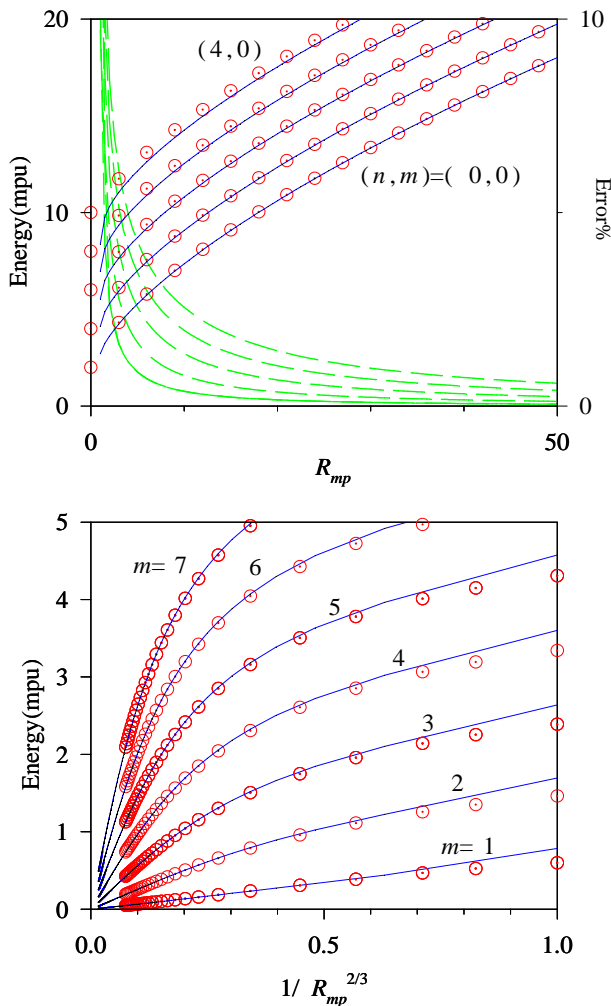


FIG. 4: (Color online) Upper panel: $\tilde{\epsilon}_{nm}$ exact energies and the analytical prediction of the roto-vibrational model (thin solid curves). The dashed lines give the relative error in percentage (right scale) with bottom to top curves corresponding to $n = 0, 1, \dots, 4$, respectively. Lower panel: Excitation energies of the $(0, m)$ states, i.e., $\tilde{\epsilon}_{0m} - \tilde{\epsilon}_{00}$ from the exact (data) and analytical model (curves).

(typically chosen as 2 or 3 %). The roto-vibrational coupling is defined as

$$\gamma(m) = 100 \frac{\omega_{vib}(m; R_{mp}) - \sqrt{3}}{\sqrt{3}}, \quad (12)$$

where ω_{vib} is the square-root factor in Eq. (9) and $\sqrt{3}$ is the limit of this quantity for $R_{mp} \rightarrow \infty$. Using a 3% condition the crystallization onset for each angular momentum is given by the R_{mp} value where each m curve of Fig. 5 enters the shaded region. Note that the crystallization onset moves towards higher values as the angular momentum is increased, reflecting the property that roto-vibrational coupling is stronger for high- m states. It is also worth mentioning that, since not all m -states are simultaneously crystallized, in practice the *rotational*

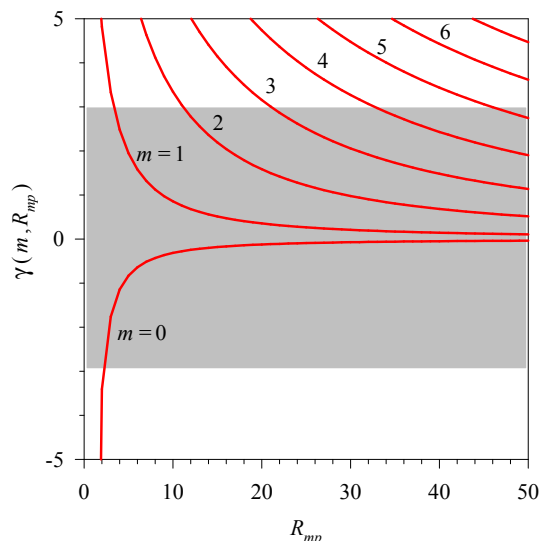


FIG. 5: (Color online) Roto-vibrational coupling as defined in Eq. (12). The shaded region indicates the crystallized phase with the criterion $\gamma \leq 3$.

bands will gradually degrade for increasing m 's as a consequence of the roto-vibrational coupling. In agreement with the bulk gas situation, the crystallized states with the proposed criterion are characterized by having a potential energy that largely exceeds the kinetic one, as can be easily checked from Eq. (9).

The crystallization properties of m and $-m$ states are identical since one can easily check that $u_{nm}(r; R_{mp}) = u_{n-m}(r; R_{mp})$. Therefore, taking into account the variations in ground state angular momentum we can draw the boundaries for Wigner crystallization in the $R_{mp} - W_{mp}$ plane, i.e., the crystallization phase diagram (see the lower panel of Fig. 2). Of course, if instead of a 3% threshold for roto-vibrational decoupling one chooses a different value the crystallization onset will vary, although as shown in Fig. 5, for low m 's the crystallization is not crucially dependent on the precise percentage in the range 2 to 4%. Actually, it should be more appropriate to speak of crystallization onset for a given percentage of roto-vibrational decoupling than of an absolute value.

It should be noted that the onset of Wigner crystallization may be studied by means of the conditional probability distribution (CPD, cf. Refs. 10,26) for finding one electron at position \mathbf{r}_1 given that the second electron is at position \mathbf{r}_2 . As soon as the interaction is switched on, the CPD, which for a system with only two electrons is just the modulus squared of the wave-function $|\Psi(\mathbf{r}_1, \mathbf{r}_2)|^2$, exhibits the formation of a molecular-like state (see Fig. 6). It is difficult, however, to use this measure alone as a conclusive evidence of the formation of the Wigner molecule in two-electron dots. The difficulty arises from the fact that even weak interactions, for which we should not expect a crystallization, yield the formation of a hole around the electron at \mathbf{r}_2 (the correlation hole) and a maximum at $\mathbf{r}_1 = -\mathbf{r}_2$. Indeed, as seen from Fig. 6, the

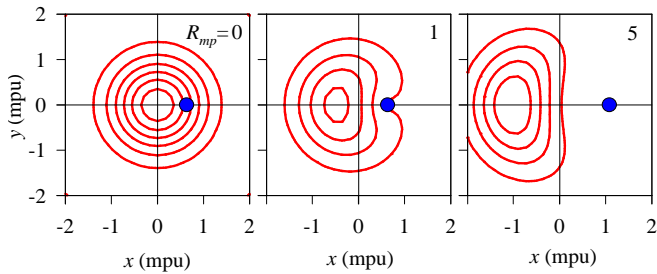


FIG. 6: (Color online) Contour plots of the ground state two-electron wave function $|\Psi(\mathbf{r}_1, \mathbf{r}_2)|^2$ for the fixed value of \mathbf{r}_2 shown by a solid symbol. A value of $W_{mp} = 0$ and the displayed R_{mp} have been used for the different panels. For $R_{mp} = 0$, \mathbf{r}_2 has been arbitrarily fixed on the x axis, while for $R_{mp} > 0$ it has been placed at the distance inferred from the asymptotic law $x_2 = r_0/2$ (see text).

results for $R_{mp} = 1$ hint at a molecular state even though according to our analysis the roto-vibrational coupling is still strong and this state is not associated with a crystallized phase (see Fig. 5). When R_{mp} increases the depletion of the CPD around the fixed electron becomes much stronger, which is in qualitative agreement with the crystallization trend from our analysis.

V. HARTREE-FOCK AND RPA APPROACHES

In this section we discuss the results obtained within the symmetry unrestricted Hartree-Fock method for the ground state and the corresponding RPA for excitations. We recall that the HF and RPA approaches were devised for the analysis of many-body systems. Therefore, their application to a two-electron quantum dot is merely an exploratory approach to the qualitative features of the Wigner crystallization rather than a quantitative description of the above exact results.

We have solved the HF problem in the Fock-Darwin basis which diagonalizes the square bracket in Eq. (1), namely $\{|a\eta\rangle; a = 1, \dots, \mathcal{N}; \eta = \uparrow, \downarrow\}$, where a labels the orbital part and η the spin. Our basis has been optimized such a way that we consider the 70 lowest Fock-Darwin states, of the non-interacting energy level scheme, for a chosen value of the magnetic field. An arbitrary single-particle orbital $|i\rangle$ is then expanded as $|i\rangle = \sum_{a\eta} B_{a\eta}^{(i)} |a\eta\rangle$. In the chosen basis, the HF equations are written as a system of nonlinear eigenvalue equations for the matrix of B coefficients (see, for instance, details in Ref. 11).

We have imposed good s_z HF orbitals leaving totally unspecified the remaining spatial symmetries. Note that the Slater determinant built with these single-particle orbitals will be an eigenstate of the total S_z operator but not, in general, of \mathbf{S}^2 . This, as we shall see in the results, is intimately connected with the prediction of broken circular symmetry.

In Fig. 7 we show the HF phase diagram in the

$R_{mp} - W_{mp}$ plane (lower panel) and the corresponding total energies (upper panel). The total energies resemble those obtained in the exact treatment, with approximate piecewise linear regions between orbital angular momentum transition lines. As expected the actual values at a given point in the diagram lie slightly above the corresponding exact results. In the lower panel different gray regions reflect a measure²⁷ of the deviation from circularity of the ground state density, with the lightest intensity corresponding to a circular (nonbroken symmetry) solution and more intense gray levels to noncircular (broken symmetry) results. The contour lines show the total orbital angular momentum L_z . Regions I and III are of circular symmetry and for them L_z has a good quantum number, taking the values 0 and -1, respectively. For the rest of the diagram (regions II, IV and V) the contour lines only indicate the expectation value of L_z but, since the mean field is not circularly symmetric, this is no longer a good quantum number. The dotted curve separates the states having total spin projection $S_z = 0$ (below) from $S_z = 1$ (above).

For $S_z = 0$ configurations, the HF method predicts a broken-symmetry solution when R_{mp} exceeds a value $\simeq 1$, somehow below the onset of crystallization obtained in Sec. IV ($R_{mp} \simeq 2.2$). In this region (II) the HF solution is indeed a mixture of singlet and triplet states, as can be verified by computing the total spin dispersion $\Delta\mathbf{S}^2$. The corresponding spatial density is built from two opposite and localized single electron orbitals. It is instructive to compare the HF solutions in region II with those obtained using a total-spin conserving ansatz

$$\Psi_{sng}(\mathbf{r}_1, \mathbf{r}_2, \eta_1, \eta_2) = \phi(\mathbf{r}_1)\phi(\mathbf{r}_2) \chi_{sng}(\eta_1, \eta_2) \quad (13)$$

$$\Psi_{trp}(\mathbf{r}_1, \mathbf{r}_2, \eta_1, \eta_2) = \mathcal{A}[\phi_1(\mathbf{r}_1), \phi_2(\mathbf{r}_2)] \times \chi_{trp}(\eta_1, \eta_2) \quad (14)$$

for singlet (Ψ_{sng}) and triplet (Ψ_{trp}) states, where $\mathcal{A}[\phi_1(\mathbf{r}_1), \phi_2(\mathbf{r}_2)]$ denotes the antisymmetrized product of the two orbitals ϕ_1 and ϕ_2 while the χ 's are the well known singlet and triplet spin states.

As a sample result the total energies obtained for $(W_{mp}, R_{mp}) = (0, 2)$ are $E_{exact} = 3.720$, $E_{HF} = 4.034$, $E_{sng} = 4.185$ and $E_{trp} = 4.168$; i.e., by requiring total \mathbf{S}^2 conservation the mean field energy raises considerably. In addition, while the HF solution breaks circular symmetry, both Ψ_{sng} and Ψ_{trp} yield circular densities because of the spatial dependence of the ϕ 's in Eqs. (13) and (14). We have also checked that these results are equivalent to those obtained using the Lipkin-Nogami projection method^{28,29} for the effective Hamiltonian $H_{eff} = \mathcal{H} - \lambda\mathbf{S}^2$ in order to restore \mathbf{S}^2 symmetry approximately. The above ansatz for states with good total spin are examples of the use of *constraints* in mean field approaches, which necessarily raise the energy above the mean field minimum. One could also project the symmetry-unrestricted HF orbitals as discussed in Ref. 30. In the latter case, however, the wave function is no longer a single Slater determinant but rather a sum of few determinants of

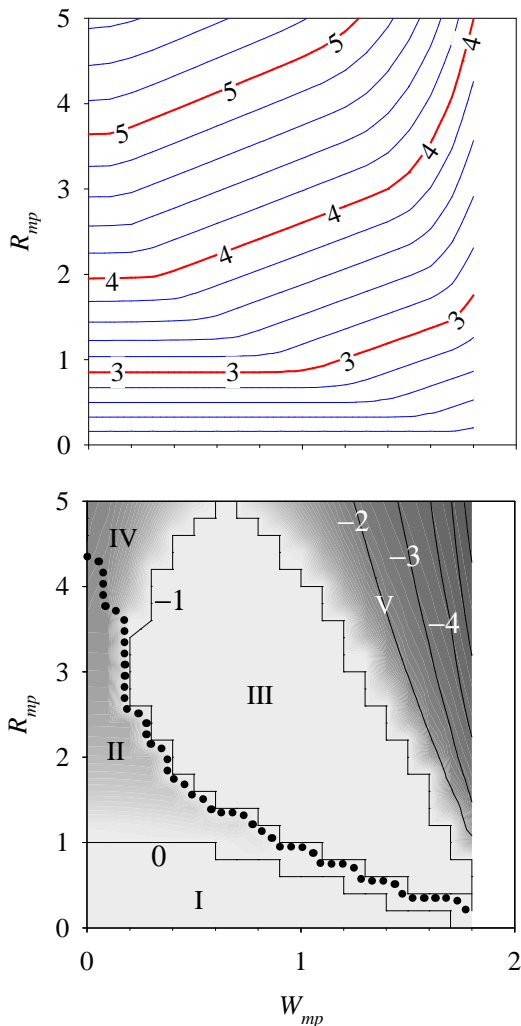


FIG. 7: (Color online) Upper panel: HF ground state energy in mpu's for the two electron dot. Lower panel: Regions (I to V) of the HF ground state phase diagram. The dotted curve separates total $S_z = 0$ (below) and $S_z = 1$ (above) configurations. The gray scale denotes the space symmetry of the HF solution,²⁷ from circular (light gray) to strongly deformed (dark gray) configurations. Labeled contour lines display $\langle L_z \rangle$. Note that in the broken-symmetry regions (II, IV and V) this latter quantity varies continuously between the integer boundaries. Results for $W_{mp} > 1.8$ are not shown due to the difficulty in determining the single-particle basis when the Fock-Darwin states become quasi-degenerate.

the corresponding symmetry operator. Therefore, the ground state energy with the restored symmetry is no longer bound by the mean-field minimum and thus can be closer to the absolute minimum imposed by the variational principle.

With the above results, we conclude that the lowest HF solution in region II requires a simultaneous breaking of the spin and space symmetries. Taking into account the results of the preceding sections we can say that singlet-triplet mixing in region II is an artifact of the HF solu-

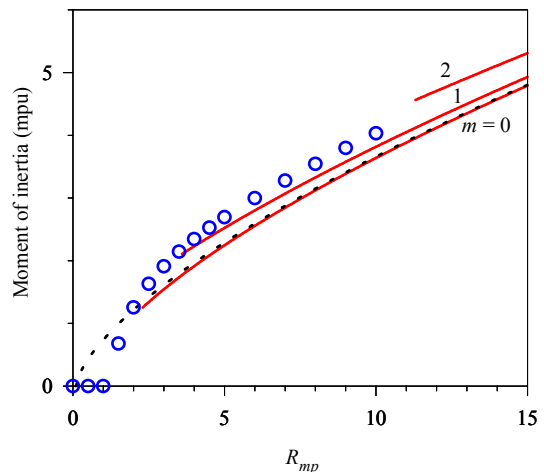


FIG. 8: (Color online) Moment of inertia computed in the RPA (circles) at $W_{mp} = 0$ as a function of the adimensional parameter R_{mp} . Solid lines show the evolution of the corresponding values in the analytical model of Sec. III for different m -states. Each line starts at the crystallization onset for the corresponding angular momentum, according to the criterion of Sec. IV.B. The dashed line represents the asymptotic value $\mathcal{J} = r_0^2/2$ taking $r_0 \approx (2R_{mp})^{1/3}$, to which all solid lines converge at very high values of R_{mp} .

tion. However, space symmetry breaking in this region is a true physical mechanism indicating an intrinsic structural change in the exact wave function, as supported by the roto-vibrational model discussed above. We believe this peculiar combination of artifact and physics is due to the smallness of the configuration space for a two-electron system. We must also point out that at high R_{mp} and/or W_{mp} (regions IV and V) the HF prediction fails to match the results of the analysis given in Sec. IV.

In contrast to the exact results of Fig. 2 where a region (although narrow) with $m = -2$ corresponding to a singlet state appears at large W_{mp} , the HF approximation predicts only one ($S_z = 0$) \rightarrow ($S_z = 1$) transition as W_{mp} increases. This can be understood as an overestimation of the exchange energy in the HF model which tends to favor spin alignment whenever orbital overlapping occurs, as it does in region III with circular orbitals, as well as in regions IV and V with two-lobed orbitals.

We consider next the results obtained by solving the RPA for excitations. As discussed in Ref. 11 the RPA determines the moment of inertia associated with the collective rotation of a deformed HF structure (see Eq. (18) in Ref. 11). Figure 8 presents the evolution with R_{mp} , at $W_{mp} = 0$, of the RPA moment of inertia \mathcal{J}_{RPA} (circles). For comparison, the values computed through the solution of Eq. (7) of the roto-vibrational model, $\mathcal{J} = r_0^2/2$, are also shown (solid lines). Each \mathcal{J} -line starts at the crystallization onset for the corresponding angular momentum using the criterion of Sec. IV.B. Note that \mathcal{J}_{RPA} remains null until the HF solution breaks rotational symmetry at $R_{mp} \simeq 1$, from there on it reasonably agrees

with the exact values, somehow averaging the exact results for different m 's. The molecule stretching, yielding larger r_0 's (\mathcal{J} 's) as m increases, is obviously outside the RPA. All \mathcal{J} values slowly converge to a common result with increasing R_{mp} , i.e., to an exact rigid-rotor behavior. For comparison, the dashed line represents the asymptotic value corresponding to $r_0 \approx (2R_{mp})^{1/3}$. The nice qualitative agreement between \mathcal{J}_{RPA} and \mathcal{J} is giving additional support to the above conclusion that space symmetry breaking in region II of the HF phase diagram indicates a genuine physical effect and, thus, it also supports the overall picture of a rotating Wigner molecule.

Although the RPA restores circularity on the deformed HF mean field,¹¹ associated with the L_z operator, it is not able to restore the symmetry related to \mathbf{S}^2 , since the latter one is a two-body operator which is beyond the RPA treatment of broken symmetries. A side effect of the HF spin artifact in region II is that when spin-flip bosonic pairs are included in the RPA, generalizing our previous calculation,¹¹ the correlation energy in this symmetry-broken phase is badly overestimated, i.e., it is between two and three times larger than the exact value. This does not occur, however, in the circularly symmetric regions.

Focusing now on the RPA vibron states, we must also distinguish excitations associated with spin and space (charge) degrees of freedom. While the RPA qualitatively describes all excitations in regions I and III, it fails for spin excitations in phase II. Obviously, this is due to the HF spin artifact in this region. It also fails for space excitations of phases IV and V. Finally, we end this section by pointing out that, in spite of the spin artifact of phase II, in pure triplet phases RPA reproduces the exact spin precession frequencies known from the theory of magnetic resonance.³¹ That is, a pure spin-flip state (precessional mode) is expected at the Larmor energy $\hbar\omega_{\mathcal{L}} = g^* \mu_B B = \frac{1}{2} g^* m^* W_{mp}$ mpu. Indeed, within the RPA, i.e., in the quasi-boson approximation,^{11,32} one finds

$$[\mathcal{H}, O_{\mathcal{L}}^+] = \hbar\omega_{\mathcal{L}} O_{\mathcal{L}}^+, \quad (15)$$

with the vibron operator for the Larmor mode

$$O_{\mathcal{L}}^+ = \frac{S_x + iS_y}{\sqrt{2\langle S_z \rangle}}. \quad (16)$$

In Eq. (16) $\langle S_z \rangle$ is the HF expectation value of the S_z operator. In fact, the Larmor mode at $\hbar\omega_{\mathcal{L}}$ appears whenever the ground state has $\langle S_z \rangle \neq 0$ and it is normally the lowest excitation of the system.

VI. SUMMARY

We performed a systematic study of the evolution of ground and excited states of two-electron quantum

dots subject to an external magnetic field. The analysis has been done in terms of magneto-parabolic units and the associated parameters (R_{mp}, W_{mp}) that give, respectively, the ratios of Coulomb interaction strength and cyclotron frequency to effective confinement. The ground state calculations are summarized in a phase diagram that can be equally applied to a variety of confinements, magnetic fields and material parameters.

We suggested an analytical model for the interpretation of the exact results, including roto-vibrational coupling and centrifugal distortion (molecule stretching). Within this roto-vibrational model we proposed a criterion to determine the onset of Wigner crystallization based on the decoupling of rotational and vibrational motions. For a 3%-decoupling threshold we found that Wigner crystallization appears, for zero-angular-momentum states, when R_{mp} exceeds a value $\simeq 2$. States with larger m 's crystallize at higher R_{mp} values. In agreement with the homogeneous gas situation the potential energy of the crystallized states is much larger than the kinetic energy, the latter one being solely due to the vibrational zero-point motion of the electrons.

The HF calculations predict that crystallization for $S_z = 0$ occurs when $R_{mp} > 1$, the new phase (II) being in an artificial mixture of singlet and triplet spin states. The space symmetry breaking in phase II is a genuine physical effect but the spin mixture is an artifact due to the smallness of the configuration space for a two-electron system. Other HF symmetry-broken phases (IV and V) do not agree with the exact results. The RPA moment of inertia qualitatively agrees with the result from the roto-vibrational model, although the molecule centrifugal distortion is missed. On the other hand, the RPA produces reliable results for space (charge) excitations in regions I, II and III, as well as for spin excitations when the HF solutions possess good \mathbf{S}^2 and S_z quantum numbers (regions I and III). We would expect a broader applicability of the many-body theories (HF+RPA) for larger systems. Work along this line is in progress. In conclusion, the combined use of exact and model calculations allowed us to ascertain the existence of a rotating Wigner molecule in a two-electron dot for relatively large electron densities or, equivalently, small R_{mp} parameters.

Acknowledgments

This work was supported by Grant No. BFM2002-03241 from DGI (Spain). R. G. N. gratefully acknowledges support from the Ramón y Cajal programme (Spain).

-
- ¹ E. P. Wigner, Phys. Rev. B **46**, 1002 (1934).
- ² G. D. Mahan, *Many-Particle Physics* (Kluwer Academic/Plenum Publishers, New York, 2000).
- ³ C. C. Grimes and G. Adams, Phys. Rev. Lett. **42**, 795 (1979).
- ⁴ E.Y. Andrei, G. Deville, D. C. Glattli, F. I. B. Williams, E. Paris, and B. Etienne, Phys. Rev. Lett. **60**, 2765 (1988).
- ⁵ S. M. Reimann and M. Manninen, Rev. Mod. Phys. **74**, 1283 (2002).
- ⁶ S. M. Reimann, M. Koskinen, M. Manninen, and B. R. Mottelson Phys. Rev. Lett. **83**, 3270 (1999).
- ⁷ C. Yannouleas and U. Landman, Phys. Rev. Lett. **85**, 1726 (2000).
- ⁸ R. S. Berry, Contemp. Phys. **30**, 1 (1989).
- ⁹ H.-M. Müller and S. E. Koonin, Phys. Rev. B **54**, 14532 (1996).
- ¹⁰ C. Yannouleas and U. Landman, Phys. Rev. Lett. **82**, 5325 (1999);
- ¹¹ Ll. Serra, R. G. Nazmitdinov, and A. Puente, Phys. Rev. B **68**, 035341 (2003).
- ¹² L. Wendler, V. M. Fomin, A. V. Chaplik, and A.O. Govorov, Phys. Rev. B **54**, 4794 (1996).
- ¹³ B. Reusch and H. Grabert, Phys. Rev. B **68**, 045309 (2003).
- ¹⁴ M. Taut, Phys. Rev. A **48**, 3561 (1993); J. Phys. A: Math. Gen. **27**, 1045 (1994).
- ¹⁵ J.-L. Zhu, J.-Z. Yu, Z.-Q. Li, and Y. Kawazoe, J. Phys.: Condens. Matter **8**, 7857 (1996).
- ¹⁶ D. Pfannkuche, V. Gudmundsson, and P. A. Maksym, Phys. Rev. B **47**, 2244 (1993).
- ¹⁷ M. Wagner, U. Merkt, and A. V. Chaplik, Phys. Rev. B **45**, 1951 (1992).
- ¹⁸ F. Pederiva, C. J. Umrigar, and E. Lipparini, Phys. Rev. B **62**, 8120 (2000).
- ¹⁹ A. V. Filinov, M. Bonitz, and Yu. E. Lozovik, Phys. Rev. Lett. **86**, 3851 (2001).
- ²⁰ M. Dineykhon and R. G. Nazmitdinov, Phys. Rev. B **55**, 13707 (1997); J. Phys.: Condens. Matter **11**, L83 (1999).
- ²¹ L. Jacak, P. Hawrylak, and A. Wojs, *Quantum Dots* (Springer, Berlin, 1998).
- ²² T. Chakraborty, *Quantum Dots: A Survey of the Properties of Artificial Atoms* (North-Holland, Amsterdam, 1999).
- ²³ B. H. Bransden and C. J. Joachain, *Physics of Atoms and Molecules* (Longman Scientific & Technical, New York, 1994).
- ²⁴ Strictly speaking, this expression is not fully analytical since r_0 is determined by the algebraic Eq. (7) that, in general, we solve numerically. Nevertheless, to simplify the discussion we shall continue to call this result and also, by extension, the complete roto-vibrational model, analytical.
- ²⁵ After the submission of the paper, we became aware that in the limit of strong magnetic fields and strong interaction, when $r_0 \approx (2R_{mp})^{1/3}$, similar results for the energy levels have been obtained in A. Matulis and F. M. Peeters, Solid State Commun. **117**, 655 (2001).
- ²⁶ S. A. Mikhailov, Phys. Rev. B **66**, 153313 (2002).
- ²⁷ We have used two alternative orbital symmetry-breaking measures, $f_1 = \sum_i \langle \Delta \ell_z \rangle_i^2$ and $f_2 = \int d\mathbf{r} (\rho(\mathbf{r}) - \tilde{\rho}(r))^2$ with $\tilde{\rho}(r) \equiv \int d\theta \rho(\mathbf{r}) / (2\pi)$.
- ²⁸ H. J. Lipkin, Ann. Phys. (N.Y.), **12**, 425 (1960).
- ²⁹ Y. Nogami, Phys. Rev. B **134**, 313 (1964); Y. Nogami and I. J. Zucker, Nucl. Phys. **60**, 203 (1964).
- ³⁰ C. Yannouleas and U. Landman, J. Phys.: Condens. Matter **14**, L591 (2002).
- ³¹ C. P. Slichter, *Principles of Magnetic Resonance* (Springer, Berlin, 1990).
- ³² J. P. Blaizot and G. Ripka, *Quantum Theory of Finite Systems* (MIT, Cambridge, MA, 1986).